Electrohydrostatics of Capillary Switches

Krishnaraj Sambath and Osman A. Basaran
Dept. of Chemical Engineering, Purdue University, West Lafayette, IN 47907

DOI 10.1002/aic.14367
Published online February 2, 2014 in Wiley Online Library (wileyonlinelibrary.com)

A capillary switch is a system of two liquid drops, one sessile and the other pendant, obtained by overfilling a hole of radius R in a plate. When surface tension dominates gravity, the equilibrium shapes of the drops are spherical sections of equal radii. If the combined volume of the top V_T and bottom V_B drops exceeds $4\pi R^3/3$, the system has three equilibrium states of which two are stable. This bistability is exploited in applications by toggling the system between its two stable states. Here, we examine the effectiveness of using an electric field for toggling. Bifurcation diagrams are obtained that depict how the system's response varies with applied field strength E, and show loss of stability at turning points and the possibility of hysteresis. A phase diagram in $E-(V_T+V_B)$ space is presented to readily infer when an electric field is an effective means for toggling. © 2014 American Institute of Chemical Engineers *AIChE J*, 60: 1451–1459, 2014

Keywords: double droplet systems, microfluidics, charged interfaces, nonlinearity

Introduction

Single drops and bubbles, such as rain drops, water drops hanging from faucets, and bubbles in carbonated beverages, are commonplace objects of everyday life. They are also extremely useful in applications ranging from ink jet printing[1,2] to measurement of surface tension.[3,4] Consequently, their dynamics have been studied extensively for almost 200 years.[1,5,6] Double droplet or bubble systems (DDSs or DBSs) are less common in everyday life but surprisingly they too have received attention for over a century. Pioneering scientific studies of such systems can be attributed to Plateau,[7] who is widely known for his field defining work on surface tension driven instabilities, and Boys.[8] Indeed, Boys can even be credited with having popularized DDSs and DBSs by carrying out public demonstrations of some of their remarkable responses to audiences consisting of juveniles in the late 1800s. In these demonstrations, Boys showed that when a valve in a tube connecting two tubes from each of which a gas bubble, surrounded by an ambient liquid, is pendant is opened so that the two bubbles become connected, the larger bubble may grow at the expense of the smaller one because the capillary pressure due to surface tension is smaller in the larger bubble compared to that in the smaller bubble. Similar observations were made by Plateau who, however, used soap bubbles rather than gas bubbles in his experiments.

More recently, there has been a resurgence of interest in DDSs owing to their occurrence in nature,[9] as well as in engineering applications where they may be used as optical lenses[10] and adhesives.[11,12] In these more recent works, a DDS, which is more commonly referred to as a capillary switch (CS), is a system of two supported drops, one sessile and the other pendant, that is obtained by overfilling with a liquid a cylindrical hole of radius $\tilde{R}$ in a plate. In the most commonly studied cases where the fluid exterior to the CS is a passive gas that exerts a constant pressure, the gravitational Bond number N_G, which measures the relative importance of gravitational force compared to surface tension force, is vanishingly small, and the two drops are pinned at their contact lines to the sharp edges of the cylindrical hole, the equilibrium shapes of the two drops are sections of spheres having the same radii of curvature. As shown by Hirsa et al.,[13] when the combined volume of the top $\tilde{V}_T$ and the bottom $\tilde{V}_B$ drops is less than $4\pi\tilde{R}^3/3$, there is only one equilibrium state, which is stable, where both drops have the same volume (cf. Figure 1). As also shown by Hirsa and coworkers, if, however, $\tilde{V}_T+\tilde{V}_B > 4\pi\tilde{R}^3/3$, there are three equilibrium states (cf. Figure 1). One of these states corresponds to an unstable equilibrium shape and is such that the two drops have the same volume. The other two states correspond to stable equilibrium shapes and are mirror images of one another such that the top (bottom) big drop is the complementary spherical section of the bottom (top) small drop. Hirsa and coworkers experimentally demonstrated that coupled water droplets can be "toggled" from one of these stable states to the other by an ambient pressure pulse.

An important challenge in many of the newer applications with CSs is to devise a means that is reliable, has a fast response, and is energy efficient to toggle the switch between its two stable states. Previously studied means for toggling include pressure excitations,[13] electrochemical excitations,[14] electroosmotic excitations,[15] and magnetic field-induced excitations to toggle CSs composed of ferrofluids.[16,17] Both from the standpoint of toggling and because of its intrinsic importance in fluid mechanics, researchers have also studied the oscillations of such coupled droplet systems. Theisen et al.[18] and Slater et al.[19] have used

Correspondence concerning this article should be addressed to O. A. Basaran at obasaran@purdue.edu.

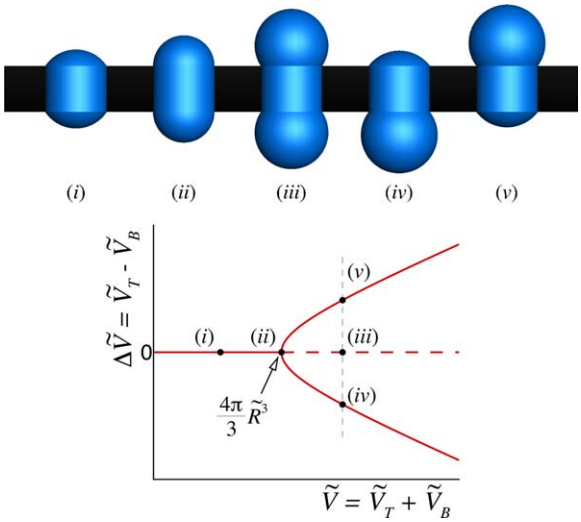

Figure 1. A CS with fixed contact lines in the limit of zero gravitational Bond number.

Top: selected equilibrium shapes, (*i*)−(*v*). Bottom: bifurcation diagram that identifies the various equilibrium states of the system by depicting the variation of the difference in volume between the top and the bottom drops, $\Delta\tilde{V} \equiv \tilde{V}_T - \tilde{V}_B$, as a function of the sum of the two volumes, that is, the total volume, $\tilde{V} \equiv \tilde{V}_T + \tilde{V}_B$. The location of each equilibrium shape shown on top is identified in the bifurcation diagram below where equilibrium shapes that lie along curves drawn as thick solid lines are stable and ones that lie along curves drawn as thick dashed lines are unstable. State (*i*) represents a stable equilibrium shape for which $\tilde{V} < 4\pi\tilde{R}^3/3$ and $\Delta\tilde{V} = 0$. State (*ii*) corresponds to a neutrally stable shape for which $\tilde{V}$ equals the critical value $4\pi\tilde{R}^3/3$ and $\Delta\tilde{V} = 0$. Although there is only a single equilibrium state when $\tilde{V} \leq 4\pi\tilde{R}^3/3$, there are three equilibrium states for each value of the total volume $\tilde{V}$ exceeding the critical volume. For CSs of volume larger than this critical value, the equivolume ($\Delta\tilde{V} = 0$) configuration (*iii*) is an unstable equilibrium state, whereas the two unequal volume ($\Delta\tilde{V} \neq 0$) configurations (*iv*) and (*v*) represent stable equilibrium states. [Color figure can be viewed in the online issue, which is available at wileyonlinelibrary.com.]

lumped parameter models to study the nonlinear oscillations of CSs. Also, a number of authors have used both analytical and numerical methods to determine the eigen modes and eigen frequencies of linearized axisymmetric oscillations of CSs of both inviscid and viscous fluids.[20–24] In this article, we examine the effectiveness of using an electric field to toggle a CS between such two states by determining as a function of the applied field strength the axisymmetric shapes and stability of a CS which is composed of a perfectly conducting liquid and where the ambient fluid is a passive dielectric gas.

Calculating the shapes and stability of a CS or for that matter of any other interfacial system such as, for example, a drop, bubble, and liquid bridge in the presence of an electric field requires that one solve the augmented Young–Laplace equation for the interface profile, which is the requisite force balance at the interface between surface tension, electric, and gravitational forces, and the Laplace equation for the electric potential in the surrounding dielectric medium. Interest in the deformation of drops and bubbles with increasing electric field strength and the onset of instability of such systems when the field strength exceeds a critical value can be traced to the experimental works carried out almost a century ago by Zeleny[25] who studied electrified drops pendant from a charged nozzle and Wilson and Taylor[26] who studied electrified soap bubbles sessile on the bottom plate of a charged parallel plate capacitor. These pioneering works with supported drops and bubbles, and also later ones with free drops by Nolan[27] and Macky,[28] showed that a conducting drop or a bubble subjected to an external electric field takes on a prolate shape in the direction of the applied field prior to becoming unstable. Before the advent of modern computers and computational methods, it was prohibitively difficult to solve the augmented Young–Laplace and Laplace equations. In what is now recognized as a landmark article, Taylor[29] circumvented these challenges while solving for the shape of a perfectly conducting drop in an imposed electric field by developing the so-called two-point approximation in which he assumed that the drop shape is identically a spheroid and satisfied the augmented Young–Laplace equation at only two specific points, the pole and the equator, on the surface of the spheroid. A related approximation was later developed by Borzabadi and Bailey[30] who relaxed the assumption that drop profiles be spheroidal shapes but achieved a simplification in which they decoupled the solution of the drop shape and electric field problems by assuming *a priori* the charge density along the drop surface. In the early 1980s, three research groups independently developed distinct numerical methods for determining the axisymmetric equilibrium shapes and stability of electrified drops without having to resort to any simplifying assumptions as in previous works.[31–33] Soon after the publication of these articles, Basaran and Scriven,[34] using the finite element-based methods developed by Basaran and Scriven,[32] carried out a detailed study of the axisymmetric shapes and stability of electrified conducting drops that are sessile on or pendant from a plate. These authors also corroborated some of their numerical results by demonstrating excellent agreement between the simulations and both new experiments on soap bubbles that they carried out and also the old experiments by Wilson and Taylor.[26] Subsequently, Wohlhuter and Basaran used methods similar to ones used by Basaran and Scriven to study the axisymmetric shapes and stability of pendant and sessile linearly[35] as well as nonlinearly[36] polarizable dielectric drops that are surrounded by a dielectric ambient fluid. Harris and Basaran[37,38] extended the earlier works by studying the axisymmetric shapes and stability of electrified drops hanging from a capillary tube for the situations in which a conducting pendant drop is surrounded by a dielectric ambient fluid and a dielectric pendant drop is surrounded by a conducting ambient fluid, respectively.

The layout of the remainder of the article is as follows. Problem Formulation section presents the augmented Young–Laplace and Laplace equations and the boundary conditions governing the shape of an electrified CS and the electric potential distribution in the ambient dielectric fluid exterior to it. Numerical Methods and Ranges of Parameters Considered section provides a brief summary of the numerical methods used to solve the governing equations along with certain validation tests that have been carried out to verify the correctness and accuracy of the algorithm used. Results and Discussion section presents a number of results including bifurcation diagrams that identify stable and unstable solutions in the governing space of parameters. The article ends with conclusions and some ideas for future work.

Problem Formulation

The system is isothermal and consists of a CS that is obtained by overfilling with a liquid of constant density ρ a cylindrical hole of radius $\tilde{R}$ in a horizontal, circular, conducting plate M that is grounded and has thickness $\tilde{L}_M$, as shown in Figure 2. Located a distance $\tilde{L}_T$ above and a distance $\tilde{L}_B$ below M are two additional conducting plates, each parallel to and concentric with plate M. Unless otherwise indicated, the top plate T is connected to a high voltage power supply so that its potential $\tilde{\Phi}_0$ can be varied, whereas the bottom plate B is grounded. The three plates have identical radii that are much larger than $\tilde{R}$ and share a common vertical axis S_S with the hole in plate M such that S_S is parallel to the gravitational acceleration **g**. The plates fit snugly inside a vertical, insulating cylindrical annulus of inner radius equal to the radii of the three plates. The region Ω_T exterior to the top drop, referred to herein also as the sessile drop, is occupied by a dielectric gas of permittivity ε_T that exerts a constant pressure $\tilde{P}_T$ on the sessile drop. The region Ω_B exterior to the bottom drop, referred to herein also as the pendant drop, is occupied by a dielectric gas of permittivity ε_B that exerts a constant pressure $\tilde{P}_B$ on the sessile drop. The surface tension of the interface S_T separating the sessile drop from the surrounding gas occupying Ω_T is denoted by γ_T and that of the interface S_B separating the pendant drop from the surrounding gas occupying Ω_B is denoted by γ_B, where both γ_T and γ_B are constants. Thus, unless otherwise indicated, an electric field $\tilde{\mathbf{E}}$ exists only in Ω_T and acts on the sessile drop. At large distances $\tilde{L}_\infty$ from the symmetry axis S_S, the electric field approaches a uniform field of strength $\tilde{\Phi}_0/\tilde{L}_T$. In certain situations (see below), once the sessile drop has been deformed sufficiently by the electric field, the top plate T is grounded and the bottom plate B is connected to the power supply so that the electric field exists only in Ω_B and acts solely on the pendant drop.

In this work, it proves convenient to use a cylindrical coordinate system $(\tilde{r}, \theta, \tilde{z})$ with its origin located at the center of the circular contact line that the sessile drop makes with the hole in plate M and where $\tilde{r}$ is the radial coordinate, $\tilde{z}$ is the axial coordinate that runs along S_S or in the direction opposite to **g**, and θ is the usual angle measured around the $\tilde{z}$ axis. Furthermore, the equilibrium shapes of CSs are taken to be axisymmetric so that the problem is independent of θ. With this simplification, the physical domain is reduced from fully three-dimensional (3-D) to 3-D but axisymmetric in the $(\tilde{r}, \tilde{z})$ plane. In what follows, the mathematical statement of the problem governing the equilibrium shapes and stability of electrified CSs is presented in dimensionless form by introducing the following scales: $l_c \equiv \tilde{R}$ as characteristic length, $p_c \equiv \gamma_T/\tilde{R}$ as characteristic pressure, and $\Phi_c \equiv \tilde{\Phi}_0$ as characteristic electric potential. In the remainder of the article, variables without tildes over them are the dimensionless counterparts of those with tildes, for example, $r \equiv \tilde{r}/\tilde{R}$ and $z \equiv \tilde{z}/\tilde{R}$.

In the electrostatic limit that applies in this article in which magnetic field effects are negligible,[39] the electric field **E** can be expressed as the negative of the gradient of a scalar electric potential Φ, viz. $\mathbf{E} = -\nabla\Phi$ and Maxwell's equations reduce to Laplace's equation for the electric potential in the region exterior to the sessile drop

$$\nabla^2\Phi = 0 \quad \text{in } \Omega_T \tag{1}$$

Here, $\Phi \equiv \tilde{\Phi}/\tilde{\Phi}_0$, $\nabla \equiv \tilde{R}\tilde{\nabla}$, and $\mathbf{E} \equiv \tilde{\mathbf{E}}/(\tilde{\Phi}_0/\tilde{R})$.

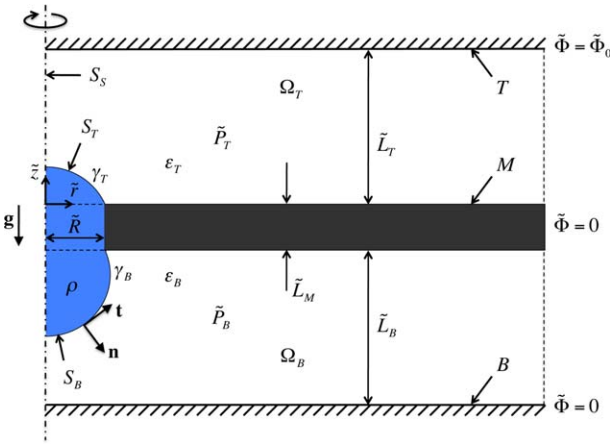

Figure 2. An electrified CS: definition sketch.

[Color figure can be viewed in the online issue, which is available at wileyonlinelibrary.com.]

Equation 1 is solved subject to a mixture of Dirichlet and Neumann boundary conditions. The Dirichlet boundary condition $\Phi = 1$ is imposed along the top plate T and the Dirichlet boundary condition $\Phi = 0$ is imposed along both plate M and the surface of the sessile drop S_T. The Neumann boundary condition $\mathbf{n} \cdot \nabla\Phi = 0$ is imposed along S_S or the z axis ($r = 0$) from the drop surface to the top plate on account of axial symmetry. The Neumann boundary condition $\mathbf{n} \cdot \nabla\Phi = 0$ is also imposed at a large but finite radial distance $r = L_\infty (\equiv \tilde{L}_\infty/\tilde{R})$ for $0 \le z \le L_T (\equiv \tilde{L}_T/\tilde{R})$ to enforce the requirement that the electric field asymptotically approaches the parallel plate field at large radial distances from the sessile drop. The outward pointing normal **n** equals $-\mathbf{e}_r$ on S_S and $+\mathbf{e}_r$ on the asymptotic boundary located at $r = L_\infty$, where $\mathbf{e}_r$ is the unit vector in the r direction.

The profiles of the sessile and the pendant drops are unknown *a priori* and vary as the field strength is varied. The equilibrium shapes of the sessile and the pendant drops are governed by the augmented Young–Laplace and Young–Laplace equations, respectively, which are the requisite balances of forces at the two interfaces

$$-2\mathcal{H} = K - N_G z + N_E L_T^2 E^2 \quad \text{on } S_T \tag{2}$$

$$-2\mathcal{H}\eta = K - \Delta P_{BT} - N_G z \quad \text{on } S_B \tag{3}$$

where $-2\mathcal{H} \equiv -2\tilde{\mathcal{H}}\tilde{R} = \nabla_s \cdot \mathbf{n}$ is twice the dimensionless local mean curvature, $\nabla_s \equiv \tilde{R}\tilde{\nabla}_s$ is the dimensionless surface gradient operator, and **n** is the unit outward normal to the interface. Here, $\eta \equiv \gamma_B/\gamma_T$ is the ratio of the surface tension of interface S_B to that of interface S_T, $K \equiv (\tilde{P}_0 - \tilde{P}_T)/(\gamma_T/\tilde{R})$ is the so-called (dimensionless) reference pressure where $\tilde{P}_0$ is the pressure in the sessile drop evaluated at the reference plane $\tilde{z} = 0$, and $\Delta P_{BT} \equiv (\tilde{P}_B - \tilde{P}_T)/(\gamma_T/\tilde{R})$ is the dimensionless pressure difference between the gas phase in the top chamber and that in the bottom chamber. The two other dimensionless groups in these equations are the gravitational Bond number $N_G \equiv \rho g \tilde{R}^2/\gamma_T$, which measures the relative importance of gravitational to surface tension force, and the electrical Bond number $N_E \equiv \varepsilon_T(\tilde{\Phi}_0/\tilde{L}_T)^2/(2\gamma_T/\tilde{R})$, which measures the relative importance of electrical to surface tension force. The electrical Bond number is defined in terms of the parallel plate field strength $E_c \equiv \tilde{\Phi}_0/\tilde{L}_T$, as it gives the right scale for the strength of the characteristic electric stress $\frac{1}{2}\varepsilon_T E_c^2$ acting on the surface of the sessile drop. The

additional term $N_E L_T^2 E^2$ in Eq. 2 accounts for the effect of the electric field on the sessile drop.

The augmented Young–Laplace and Laplace equations require two boundary conditions each. First, both equations are solved subject to pinned or fixed contact line boundary conditions, which are imposed as Dirichlet boundary conditions, where each drop meets the sharp edge of the cylindrical hole. Second, both equations are subject to boundary conditions that enforce axial symmetry of the drop profiles, which are imposed as Neumann boundary conditions at the drop tips located at $r = 0$.

Although ΔP_{BT}, along with N_G and N_E, is a specified parameter, K is also unknown *a priori* and is determined by solving a volume constraint along with Eqs. 1–3

$$V_T + V_B = V \tag{4}$$

where $V_T \equiv \tilde{V}_T/\tilde{R}^3$ and $V_B \equiv \tilde{V}_B/\tilde{R}^3$ are the dimensionless volumes of the sessile and the pendant drops and $V \equiv \tilde{V}/\tilde{R}^3$ is the dimensionless total volume of liquid contained in the CS excluding the dimensionless volume of liquid πL_M, where $L_M \equiv \tilde{L}_M/\tilde{R}$, held within the cylindrical hole.

Numerical Methods and Ranges of Parameters Considered

Equations 1–4, along with the aforementioned boundary conditions to which they are subject, are a set of coupled nonlinear partial differential, ordinary differential, and algebraic equations. This equation set is solved using a numerical method consisting of the Galerkin finite element method,[34] elliptic mesh generation,[40] and adaptive parameter stepping.[37] The correctness and accuracy of the algorithm has been confirmed by a number of tests including slightly modifying the new algorithm to determine the shapes and stability of pendant and/or sessile drops in an electric field and demonstrating that computational predictions made with the new algorithm are in excellent agreement with published results.[34,37]

When the relative importance of gravitational and electrical forces are vanishingly small compared to surface tension forces, both the gravitational Bond number and the electrical Bond number equal zero ($N_G = 0$ and $N_E = 0$) and the shapes of both the top and the bottom drops are sections of spheres or spherical caps. If the dimensionless radii of these sessile and pendant spherical caps are denoted by $R_T \equiv \tilde{R}_T/\tilde{R}$ and $R_B \equiv \tilde{R}_B/\tilde{R}$, respectively, then Eqs. 2 and 3 reduce to $K = 2/R_T$ and $K - \Delta P_{BT} = 2\eta/R_B$. The typical size of most MEMS devices range from a few to hundreds of micrometers. Therefore, for a CS which uses water as the working fluid and where the hole radius $\tilde{R} = 100$ μm, $N_G = 1.4 \times 10^{-3}$ such that the gravitational force is negligible compared to surface tension force. Given the insignificance of gravitational force in such small-scale CSs and in order to focus primarily on the effect of electric force on the shapes and stability of CSs, the remainder of the article is focused on situations in which $N_G = 0$, the two gas phases surrounding the CS both above and below plate M exert the same pressure so that $\Delta P_{BT} = 0$, and the surface tensions of the two liquid–gas interfaces separating the CS from the top and bottom gas phases are equal so that $\eta = 1$. With $N_G = 0$, $\Delta P_{BT} = 0$, and $\eta = 1$, $R_T = R_B$ when $N_E = 0$. Starting with a stable solution corresponding to an unelectrified CS of $R_T = R_B$, families of equilibrium solutions[34,37] of fixed volume are then computed by varying the electrical Bond number N_E. Because the CS and the middle plate M are perfectly conducting and when the electric field solely acts on the top sessile drop, L_M and $L_B \equiv \tilde{L}_B/\tilde{R}$ have no effect whatsoever on the equilibrium shapes and stability of electrified CSs. In the remainder of the article, values of $L_T = 7.5$ and $L_\infty = 7.5$ have been chosen as further increases in the values of these two geometrical parameters have been found to have a negligible effect on the computed results.

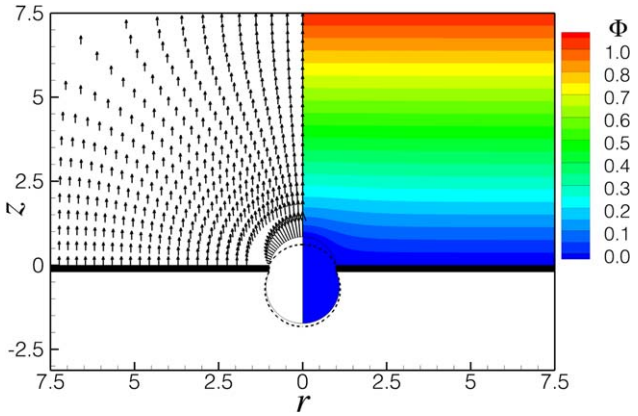

Figure 3. The effect of the electrical Bond number on the equilibrium shape of a CS of total volume $V_T + V_B = \frac{4}{3}\pi(1.12)^3$.

Here the solid curve (—) indicates the equilibrium shape of the CS when $N_E = 0.01$ and the dashed curve (- - -) indicates the equilibrium shape of the same CS in the absence of electric field, that is, when $N_E = 0$. Also shown in the figure in the region Ω_T exterior to the sessile drop when $N_E = 0.01$ are the electric field vectors to the left of the axis of symmetry S_S ($r = 0$) and the contours of electric potential to the right of S_S. The lengths of the arrows denoting the electric field vectors have been scaled relative to the maximum value of the electric field strength. Each vector shown belongs to its base point. Contour values of the electric potential are indicated by the color scale bar to the right of the figure. [Color figure can be viewed in the online issue, which is available at wileyonlinelibrary.com.]

Results and Discussion

To illustrate the response of a CS to an applied electric field, let us consider a CS of volume $V_T + V_B = \frac{4}{3}\pi(1.12)^3 = 5.89$ which in the absence of an electric field, that is, when $N_E = 0$, consists of a subhemispherical sessile drop of volume $V_T = 1.09$ and a superhemispherical pendant drop of volume $V_B = 4.80$. Figure 3 shows the shapes of the sessile and the pendant drops and also the electric field and the contours of electric potential outside the sessile drop when the CS is subjected to a weak electric field such that $N_E = 0.01$. Figure 3 makes plain that the electric field causes the sessile drop to deform in the field direction and also results in the volume of the sessile drop to increase at the expense of that of the pendant drop. As will be the case so long as the electric field solely acts on the sessile drop, it follows from Eq. 3 that $-2\mathcal{H} = K$ and, therefore, that the shape of the pendant drop should remain a section of a sphere, which has constant mean curvature K (the value of which depends on the electrical Bond number), regardless of the value of N_E. However, the profile of the sessile drop is no longer a section of a sphere due to the action of a spatially varying electric field, and hence a

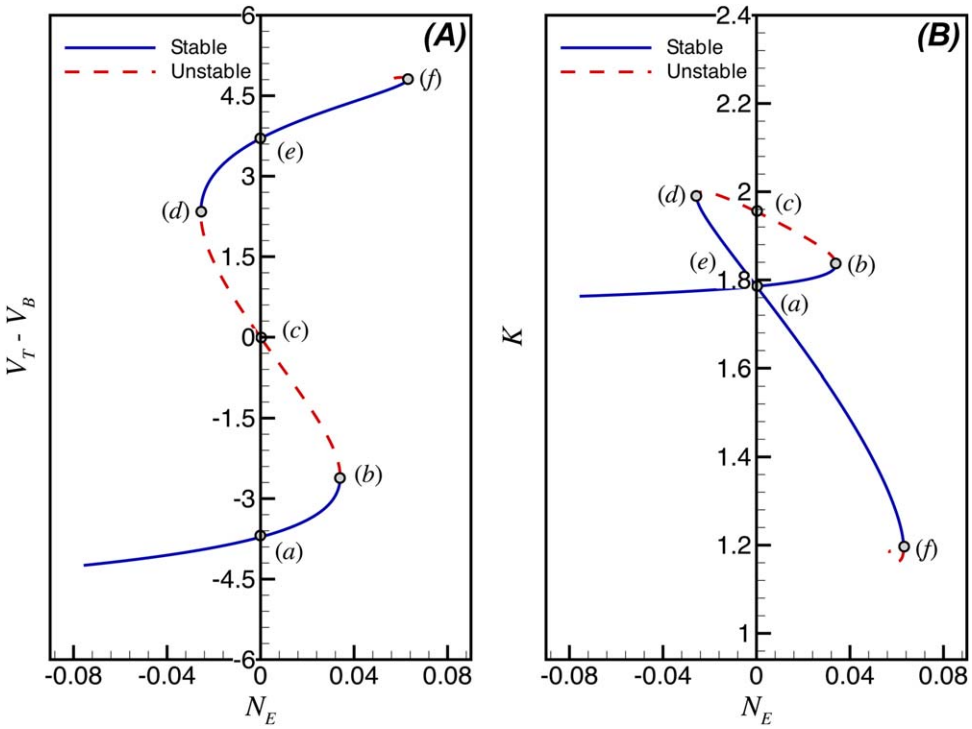

Figure 4. Bifurcation diagrams showing the evolution with the electrical Bond number N_E of a family of equilibrium shapes of a CS of volume $V_T+V_B=\frac{4}{3}\pi(1.12)^3$: variation of (*A*) the volume difference between the sessile and the pendant drops V_T-V_B with N_E and (*B*) reference pressure K with N_E.

Here, branches of stable solutions are denoted by continuous curves (—) and ones of unstable solutions are denoted by dashed curves (- - -). In both panels, equilibrium states in the absence of electric field are identified by points (*a*), (*c*), and (*e*). Also in both panels, points (*b*), (*d*), and (*f*) identify turning points where the system undergoes a change in stability. [Color figure can be viewed in the online issue, which is available at wileyonlinelibrary.com.]

spatially varying electric stress whose magnitude is proportional to the square of the strength of the local electric field, along the surface of the sessile drop. Indeed, the electric field strength (electric stress) varies from zero at the contact line ($r=1$) to its maximum value at the apex of the sessile drop ($r=0$), thereby causing the sessile drop to lose its spherical symmetry and suffer a prolate deformation in Figure 3.

The evolution of a family of equilibrium shapes of a CS of fixed volume with the strength of the applied electric field can be conveniently displayed in a bifurcation diagram where some measure of the system's response, for example, the difference between the volumes of the sessile and the pendant drops, V_T-V_B, the reference pressure K, or the aspect ratio of either drop, is plotted as a function of N_E. Figure 4(A), to be discussed first, and Figure 4(B), to be discussed below, show two such bifurcation diagrams where V_T-V_B and K, respectively, are plotted as a function of N_E for a CS of volume $V_T+V_B=\frac{4}{3}\pi(1.12)^3=5.89$. Along the *S*-shaped curve that depicts the shape family, six points of special interest are identified. Three of these points, (a), (c), and (e), correspond to equilibrium solutions when $N_E=0$. The other three, points (b), (d), and (f), correspond to turning or limits points where the slope of the *S*-shaped curve is infinite. The equilibrium shapes at all six points are shown in Figure 5. It is well known from bifurcation theory that turning points identify locations in bifurcation diagrams where a system will undergo a change of stability.[41,42] Therefore, it proves expedient in what follows to discuss the response of the CS along distinct portions of the *S*-shaped curve by dividing the curve into several segments demarcated by these points and studying each one individually. Here, the segments to be discussed consist of the branch from $(a)-(b)$, the branch $(b)-(c)-(d)$, the branch $(d)-(e)-(f)$ and finally the portions of the *S*-shaped curve lying to the left of (a) and past the upper turning point (f).

As point (a) represents a stable equilibrium state that corresponds to a CS with a subhemispherical sessile drop of volume $V_T=1.09$ and a superhemispherical drop of volume $V_B=4.80$ when $N_E=0$ (cf. Figure 5), all members of the shape family that lie along the branch $(a)-(b)$ that arise as the electric Bond number is increased from zero to its value at the turning point (b) are therefore stable. It should be noted that this stable branch, as all other stable branches, is drawn as a solid curve in the bifurcation diagram, Figure 4(A). Similarly, all members of the shape family that lie along the branch $(d)-(e)-(f)$ are stable as point (e) also represents a stable equilibrium state that, however, corresponds to a CS with a superhemispherical sessile drop of volume $V_T=4.80$ and a subhemispherical drop of volume $V_B=1.09$ when $N_E=0$ (cf. Figure 5). Conversely, all members of the shape family that lie along the branch $(b)-(c)-(d)$ are unstable because point (c) represents an unstable equilibrium state that corresponds to a CS with equivolume sessile and pendant drops of volume $V_T=V_B=\frac{2}{3}\pi(1.12)^3=2.95$ when $N_E=0$ (cf. Figure 5). It should be noted that this unstable branch, as all other unstable branches, is drawn as a dashed curve in the bifurcation diagram. As has already been stated, the turning points (b), (d), and (e) are associated with a change in the system's stability. Starting from the known stable state (a) and moving in the direction of increasing electric Bond number N_E, the *S*-shaped curve turns counterclockwise around (b) and the system loses

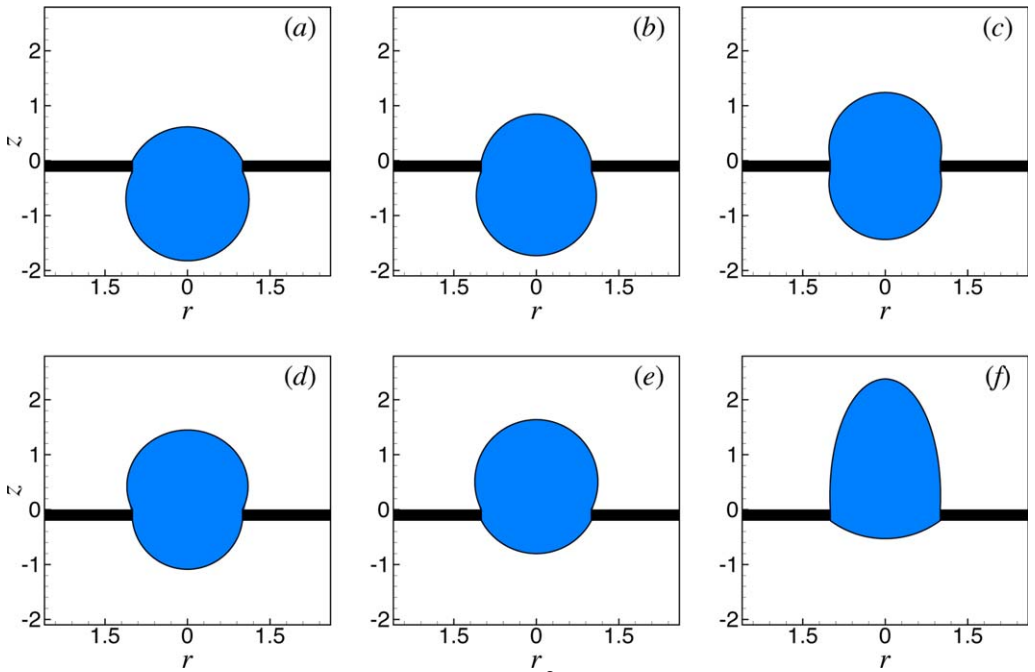

Figure 5. Equilibrium shapes of a CS of volume $V=\frac{4}{3}\pi(1.12)^3$ when $N_E=$ (*a*) 0, (*b*) 0.03, (*c*) 0, (*d*) −0.03, (*e*) 0, and (*f*) 0.06 corresponding to points (*a*) through (*f*), respectively, in Figure 4.

[Color figure can be viewed in the online issue, which is available at wileyonlinelibrary.com.]

stability. Similarly, starting from another known stable state (e) and moving in the direction of increasing electric Bond number N_E, the *S*-shaped curve again turns counterclockwise around (f) and the system once again loses stability. In contrast, starting from the known unstable state (c) and marching toward (d), the *S*-shaped curve turns clockwise around (d) and the system becomes stable once again. It should be noted that solutions obtained for values of $N_E < 0$ are not physically realizable and represent purely mathematical solutions of the governing equations that are automatically determined by the adaptive parameter stepping algorithm.

According to Figure 4(A), while $V_T - V_B < 0$ along branch $(a)-(b)$ (pendant drop being the larger of the two drops) and $V_T - V_B > 0$ along branch $(e)-(f)$ (sessile drop being the larger of the two drops), the slope of the curve $V_T - V_B$ vs. N_E is positive, that is, $d(V_T - V_B)/dN_E > 0$, along both branches implying that increasing N_E leads to the growth of the sessile drop at the expense of the pendant drop as the total volume of the CS is fixed. In other words, the electric field exerts an attractive force on the sessile drop pulling it toward the top plate and thereby causing the transfer of volume from the pendant to the sessile drop, along both branches. This behavior is further investigated using a second bifurcation diagram, Figure 4(B), where the excess pressure K within the CS over the ambient pressure is plotted as a function of N_E for the same CS as in Figure 4(A). Figure 4(B) shows that while K increases with N_E, that is, $dK/dN_E > 0$, along branch $(a)-(b)$, K decreases with N_E, that is, $dK/dN_E < 0$, along branch $(e)-(f)$. These findings can be explained by taking advantage of the fact that when $N_G=0$, the pressure is uniform within the CS and that the pressure within the sessile drop is, therefore, the same as the pressure within the pendant drop. However, the pressure within the pendant drop, K, can be readily related to its volume, and hence its radius of curvature R_B, because its equilibrium shape is always a spherical section, so that $K=2/R_B$. Along branch $(a)-(b)$, the volume of the pendant drop is always larger than that of a hemisphere, $V_B > 2\pi/3$, and

$$V_B = \frac{2\pi}{3}\left[R_B^3 + \left(R_B^2 + \frac{1}{2}\right)\sqrt{R_B^2 - 1}\right] \tag{5}$$

$$\frac{dV_B}{dR_B} = \frac{\pi R_B}{\sqrt{R_B^2 - 1}}\left(R_B + \sqrt{R_B^2 - 1}\right)^2 \tag{6}$$

$$> 0$$

Thus, as V_B decreases, R_B decreases with it along this branch. As a result, $K=2/R_B$ increases and hence $dK/dN_E > 0$ along the branch $(a)-(b)$, as shown in Figure 4(B). Conversely, along branch $(e)-(f)$, the volume of the pendant drop is always smaller than that of a hemisphere, $V_B < 2\pi/3$, and

$$V_B = \frac{2\pi}{3}\left[R_B^3 - \left(R_B^2 + \frac{1}{2}\right)\sqrt{R_B^2 - 1}\right] \tag{7}$$

$$\frac{dV_B}{dR_B} = -\frac{\pi R_B}{\sqrt{R_B^2 - 1}}\left(R_B - \sqrt{R_B^2 - 1}\right)^2 \tag{8}$$

$$< 0$$

Thus, as V_B decreases, R_B increases with it along this branch. As a result, $K=2/R_B$ decreases and hence $dK/dN_E < 0$ along the branch $(e)-(f)$, as also shown in Figure 4(B).

Incomplete hysteresis

Figure 6(A) highlights an interesting phenomenon that we shall refer to as "incomplete hysteresis" and which arises when a CS is being switched between its so-called "down state" where for $N_E=0$, the sessile drop is the smaller of the two drops and has volume $V_T \equiv V^* < 2\pi/3$ and its so-called "up state" where for $N_E=0$, the sessile drop is the larger of the two drops and the pendant drop has volume

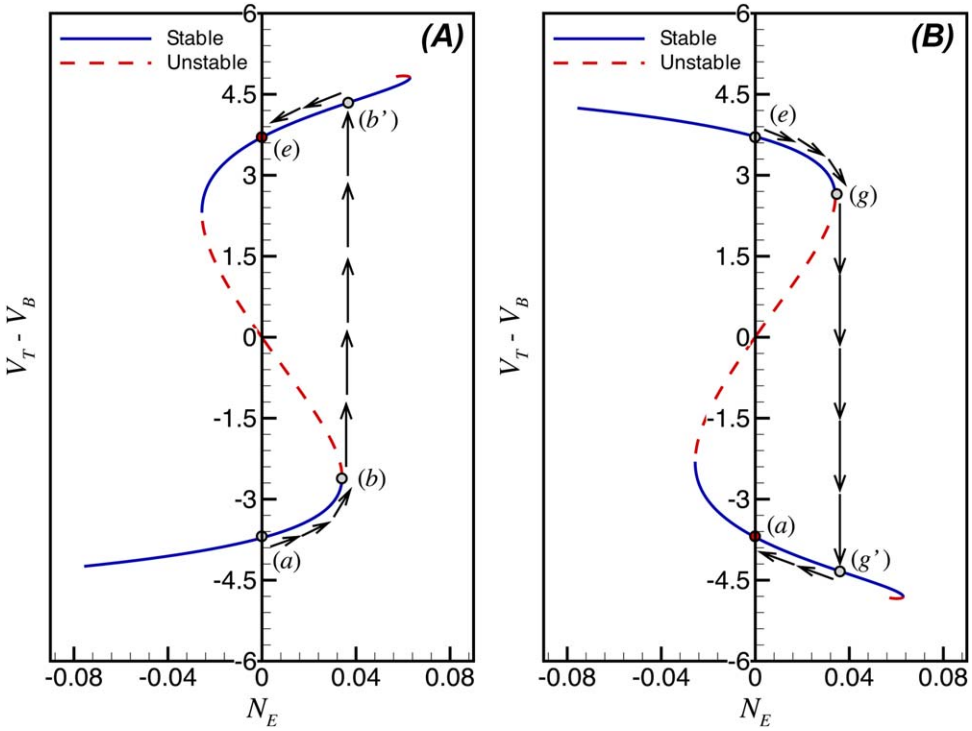

Figure 6. Bifurcation diagrams showing the variation of the volume difference between the sessile and the pendant drops $V_T - V_B$ with the electrical Bond number N_E of families of equilibrium shapes of CSs of volume $V_T + V_B = \frac{4}{3}\pi(1.12)^3$: shape family where the electric field is applied to (*A*) the sessile drop and (*B*) the pendant drop.

The arrows indicate the paths that would be followed as the CS is quasistatically switched from the down state to the up state in (*A*) and from the up state to the down state in (*B*). In both panels, branches of stable solutions are denoted by continuous curves (—) and ones of unstable solutions are denoted by dashed curves (- - -).[Color figure can be viewed in the online issue, which is available at wileyonlinelibrary.com.]

$V_B \equiv V^* < 2\pi/3$, that is, the two states are mirror images of one another about the conducting plate M. In Figure 6(A), starting at point (a)—the down state—and as the field strength or N_E is progressively increased, the system goes through a sequence of stable equilibrium states along the lower branch of stable equilibrium solutions and eventually reaches point (b)—a turning point. If the field strength or N_E were to be increased by even an infinitesimal amount beyond its value at (b), the system would jump to the equilibrium state (b') located along the upper branch of stable equilibrium solutions. Now, starting at point (b'), if the field strength or N_E is progressively decreased, the system would eventually reach point (e)—the up state where $N_E = 0$. As N_E cannot become negative in a real experiment, the system would remain stuck at (e). These results indicate that such a CS would act as a one-way switch under the action of an applied electric field. In situations where it is desirable to switch the system back to its "down" state (a), an electric field can then be applied solely in Ω_B and hence on the pendant drop, as shown in Figure 6(B). Starting at point (e), as the field strength or N_E is progressively increased, the system would then march toward turning point (g) along the upper branch and, upon an infinitesimal increase in N_E, the system would jump to the equilibrium state (g') located along the lower branch of stable equilibrium solutions. Now, starting at point (g'), if the field strength or N_E is progressively decreased, the system would eventually reach point (a) again—the down state where $N_E = 0$. It should be noted here that the actual dynamics of such switches, however, will depend on additional system parameters such as the liquid's density and viscosity.

Switchable range

Figure 7 is a bifurcation diagram that shows the evolution of several families of equilibrium shapes of CSs of different volumes with the electrical Bond number N_E. This figure makes plain that as the volumes of the CSs increase, the lower turning points shift to the right, that is, to larger values of N_E. In other words, the field strength required to deform the sessile drop and destabilize a CS increases as the sessile drop becomes smaller. This result can be readily rationalized by means of a simple scaling argument. If the electric stress that tends to deform the sessile drop is balanced against the capillary pressure due to surface tension that tends to prevent the drop from deforming, it follows that the square of the field strength times the characteristic linear dimension of the drop (e.g., the cube root of its volume) must equal a constant. Moreover, this result accords with findings of earlier studies on conducting drops that are pendant from or sessile on a solid surface which showed that the field strength required to destabilize a drop increases as the drop volume decreases.[34] By similar reasoning, the upper turning points in Figure 7 shift to the left, that is, to smaller values of N_E, as the volumes of the CSs increase as the field strength required to deform the sessile drop and destabilize a CS decreases as the sessile drop becomes larger. Therefore, as the total volume increases and the lower turning points shift to the right and the upper turning points shift to the left, a critical value

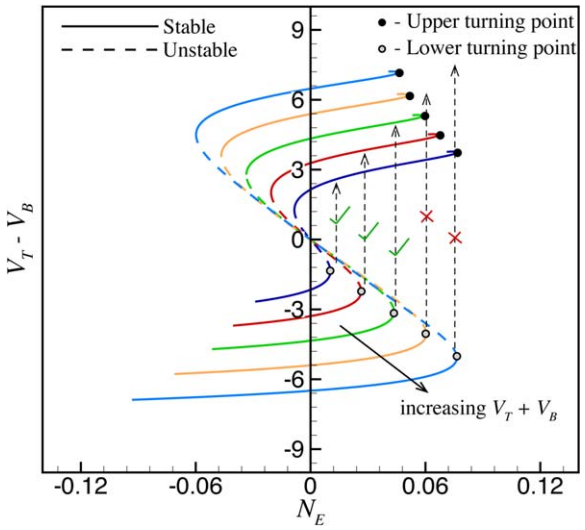

Figure 7. Bifurcation diagram showing the variation of the volume difference between the sessile and the pendant drops $V_T - V_B$ with the electrical Bond number N_E of families of equilibrium shapes of CSs of volumes of $4\pi/3$ times $(1.01)^3$, $(1.05)^3$, $(1.12)^3$, $(1.20)^3$, and $(1.25)^3$.

The upper and lower turning point along the shape families and stable and unstable branches along them are identified as per the legends in the figure. [Color figure can be viewed in the online issue, which is available at wileyonlinelibrary.com.]

of the total volume is eventually reached for which the values of N_E at the two turning points become the same. For total volumes larger than this critical value, the hysteresis phenomenon discussed in the previous section is no longer possible. Hence, there is an upper limit V_c on the total volume of a CS for which the system can be toggled from its down state to its up state using an electric field. This upper limit has been found from simulations to equal $(1.65)4\pi/3$.

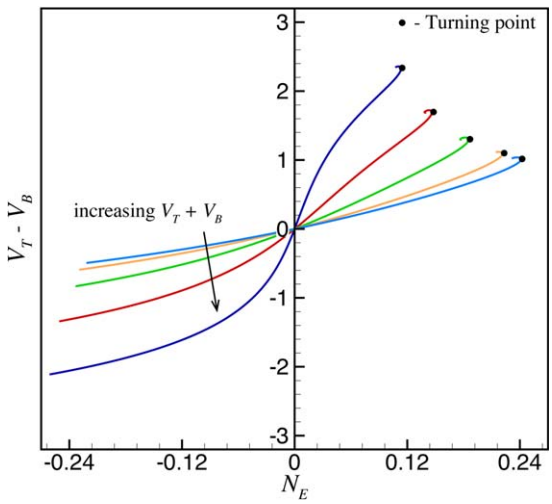

Figure 8. Bifurcation diagram for electrified capillary lenses or coupled droplets of volumes less than $4\pi/3$ that shows that such systems do not exhibit multiple stable equilibrium states.

[Color figure can be viewed in the online issue, which is available at wileyonlinelibrary.com.]

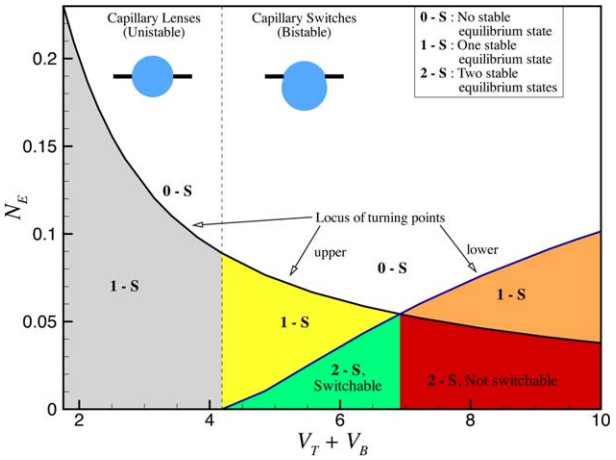

Figure 9. Phase plot in the space of the square of the dimensionless applied field strength (N_E) and the dimensionless total volume ($V_T + V_B$).

The diagram identifies loci of both the lower and upper turning points which represent values of N_E at which families of equilibrium shapes of CSs become unstable to infinitesimal-amplitude perturbations. The diagram also identifies regions of the phase space where no stable, one stable, and two stable equilibrium states exist. The phase plot shows that there exist two regions in which there are two stable equilibrium states: in one of these regions, the CS is electrically switchable, but in the other, the CS is not electrically switchable on account of the fact that the value of N_E at the lower turning point is larger than that at the upper turning point. [Color figure can be viewed in the online issue, which is available at wileyonlinelibrary.com.]

DDSs of volumes less than $4\pi/3$, referred to as capillary lenses (CLs), do not exhibit multiplicity of stable equilibrium solutions. Figure 8 is a bifurcation diagram that shows the evolution of several families of equilibrium shapes of CLs of different volumes with the electrical Bond number N_E. From Figures 7 and 8, it can be readily inferred that the lower limit on the total volume of a DDS for which the incomplete hysteresis phenomenon reported earlier can be observed is in fact the minimum volume $4\pi/3$ required for unelectrified DDSs to exhibit the sort of bistability that was discussed in Introduction. Hence, these two limits bound the range of volumes of CSs that can be toggled by means of an electric field

$$\frac{4\pi}{3} < V_T + V_B < V_c = (1.65)\frac{4\pi}{3} \tag{9}$$

Conclusions

In this article, the possibility of using an electric field to toggle a CS exhibiting bistable equilibrium states has been analyzed computationally by solving for the axisymmetric shapes and stability of DDSs that are subject to an electric field. The question of whether DDSs can be toggled and the limits of stability of such systems with respect to applied field strength are summarized in Figure 9 which is a phase diagram in the $(N_E, V_T + V_B)$ parameter space. As indicated by Eq. 9, the region shaded in green and marked as $2-S$, Switchable, in this figure represents the range of volumes over which the system exhibits bistable nature and can be toggled between its two bistable states by application of an electric field. The top boundary of this region, which

represents the locus of lower turning points, represents the minimum field strength (or, equivalently, N_E) required to achieve toggling. All other regions correspond to systems that either exhibit two stable states but are incapable of being toggled via the application of an electric field or simply do not exhibit multiple stable states.

Having identified the regions of the parameter space where an electric field can be used to quasistatically toggle a CS, future work will focus on studying the dynamic response of CSs using methods that recently have been used to study the disintegration of electrified drops.[43,44] Such studies can then be used to calculate the total time required for toggling as a function of the system properties and allow comparison of the efficacy of electric fields against other methods for toggling the system.

Acknowledgments

This work was supported by the BES program of the US DOE (DE-FG02–96ER14641). The authors also thank Dr. S. K. Ramalingam, currently at Dow Chemicals and a former member of the Drop Dynamics Research Group at Purdue University, for insightful discussions on the subject. The senior author (O.A.B.) had the privilege of being introduced to Transport Phenomena in 1975 while a sophomore at MIT by Prof. R. C. Armstrong who had just completed in 1973 his Ph.D. under the direction of Prof. R. B. Bird at the University of Wisconsin. As this course and various books authored by Prof. Bird played a major role in O.A.B.'s career as a fluid mechanician, the authors dedicate this article to Prof. Bird on the occasion of the founder's issue of the *AIChE Journal* in his honor.

Literature Cited

1. Basaran OA. Small-scale free surface flows with breakup: drop formation and emerging applications. *AIChE J*. 2002;48:1842–1848.
2. Basaran OA, Gao H, Bhat PP. Nonstandard inkjets. *Annu Rev Fluid Mech*. 2013;45:85–113.
3. Franses EI, Basaran OA, Chang CH. Techniques to measure dynamic surface tension. *Curr Opin Colloid Interface Sci*. 1996;1(2):296–303.
4. Zhang X, Harris MT, Basaran OA. Measurement of dynamic surface tension by a growing drop technique. *J Colloid Interface Sci*. 1994;168(1):47–60.
5. Eggers J. Nonlinear dynamics and breakup of free-surface flows. *Rev Mod Phys*. 1997;69:865–929.
6. Eggers J, Villermaux E. Physics of liquid jets. *Rep Prog Phys*. 2008;71:1–79.
7. Plateau J. Experimental and theoretical researches on the figures of equilibrium of a liquid mass withdrawn from the action of gravity. *Annual Report of the Board of Regents of the Smithsonian Institution*. Washington, D.C.: Government Printing Office, 1863:207–285.
8. Boys CV. *Soap Bubbles and the Forces which Mould them*. London: Society for promoting Christian knowledge, 1890.
9. Eisner T, Aneshansley DJ. Defense by foot adhesion in a beetle (*Hemisphaerota cyanea*). *Proc Natl Acad Sci USA*. 2000;97(12):6568–6573.
10. López CA, Hirsa AH. Fast focusing using a pinned-contact oscillating liquid lens. *Nat Photonics*. 2008;2(10):610–613.
11. Ward T. Electrohydrostatic adhesion of rigid-planar electrodes. *J Electrostat*. 2007;65(12):742–749.
12. Vogel MJ, Steen PH. Capillarity-based switchable adhesion. *Proc Natl Acad Sci USA*. 2010;107(8):3377–3381.
13. Hirsa AH, López CA, Latin MA, Vogel MJ, Steen PH. Low-dissipation capillary switches at small scales. *Appl Phys Lett*. 2005;86:014106.
14. López CA, Lee CC, Hirsa AH. Electrochemically activated adaptive liquid lens. *Appl Phys Lett*. 2005;87(13):134102–134102.
15. Vogel MJ, Ehrherd P, Steen PH. The electroosmotic droplet switch: countering capillarity with electrokinetics. *Proc Natl Acad Sci USA*. 2005;102:11974–11979.
16. Malouin BA Jr, Vogel MJ, Hirsa AH. Electromagnetic control of coupled droplets. *Appl Phys Lett*. 2010;96(21):214104–214104.
17. Malouin BA Jr, Vogel MJ, Olles JD, Cheng L, Hirsa AH. Electromagnetic liquid pistons for capillarity-based pumping. *Lab Chip*. 2011;11(3):393–397.
18. Theisen E, Vogel MJ, López CA, Hirsa AH, Steen PH. Capillary dynamics of coupled spherical-cap droplets. *J Fluid Mech*. 2007;580:495–505.
19. Slater DM, López C, Hirsa AH, Steen PH. Chaotic motions of a forced droplet–droplet oscillator. *Phy Fluids*. 2008;20:092107.
20. Bostwick JB, Steen PH. Capillary oscillations of a constrained liquid drop. *Phys Fluids*. 2009;21:032108.
21. Ramalingam SK, Basaran OA. Axisymmetric oscillation modes of a double droplet system. *Phys Fluids*. 2010;22:112111.
22. Ramalingam SK, Ramkrishna D, Basaran OA. Free vibrations of a spherical drop constrained at an azimuth. *Phys Fluids*. 2012;24:082102.
23. Prosperetti A. Linear oscillations of constrained drops, bubbles, and plane liquid surfaces. *Phys Fluids*. 2012;24:032109.
24. Bostwick JB, Steen PH. Coupled oscillations of deformable spherical-cap droplets. Part 2. Viscous motions. *J Fluid Mech*. 2013;714:336–360.
25. Zeleny J. Instability of electrified liquid surfaces. *Phys Rev*. 1917;10:1–6.
26. Wilson CT, Taylor GI. The bursting of soap-bubbles in a uniform electric field. *Math Proc Cambridge Philos Soc*. 1925;22(5):728–730.
27. Nolan JJ. The breaking of water-drops by electric fields. *Proc R Irish Acad Math Phys Sci*. 1924;37:28–39.
28. Macky WA. Some investigations on the deformation and breaking of water drops in strong electric fields. *Proc R Soc London Ser A*. 1931;133(822):565–587.
29. Taylor GI. Disintegration of water drops in an electric field. *Proc R Soc A*. 1964;280:383–397.
30. Borzabadi E, Bailey AG. The profiles of axially symmetric electrified pendent drops. *J Electrostat*. 1978;5:369–380.
31. Miksis MJ. Shape of a drop in an electric field. *Phys Fluids*. 1981;24(11):1967–1972.
32. Basaran OA, Scriven LE. "Profiles of electrified drops and bubbles." In *Proceedings of the Second International Colloquium on Drops and Bubbles,* JPL Publication 82-7, Dennis H. Le Croissette, ed., pp. 322–329, Jet Propulsion Laboratory, California Institute of Technology, Pasadena, CA, 1982.
33. Joffre G, Prunet-Foch B, Berthomme S, Cloupeau M. Deformation of liquid menisci under the action of an electric field. *J Electrostat*. 1982;13(2):151–165.
34. Basaran OA, Scriven LE. Axisymmetric shapes and stability of pendant and sessile drops in an electric field. *J Colloid Interface Sci*. 1990;140:10–30.
35. Wohlhuter FK, Basaran OA. Shapes and stability of pendant and sessile dielectric drops in an electric field. *J Fluid Mech*. 1992;235:481–510.
36. Basaran OA, Wohlhuter FK. Effect of nonlinear polarization on shapes and stability of pendant and sessile drops in an electric (magnetic) field. *J Fluid Mech*. 1992;244:1–1.
37. Harris MT, Basaran OA. Capillary electrohydrostatics of conducting drops hanging from a nozzle in an electric field. *J Colloid Interface Sci*. 1993;161:289–413.
38. Harris MT, Basaran OA. Equilibrium shapes and stability of nonconducting pendant drops surrounded by a conducting fluid in an electric field. *J Colloid Interface Sci*. 1995;170:308–319.
39. Melcher JR, Taylor GI. Electrohydrodynamics: a review of the role of interfacial shear stresses. *Annu Rev Fluid Mech*. 1969;1(1):111–146.
40. Notz PK, Basaran OA. Dynamics and breakup of a contracting liquid filament. *J Fluid Mech*. 2004;512:223–256.
41. Pitts E. Stability of a drop hanging from a tube. *IMA J Appl Math*. 1976;17:387–397.
42. Iooss G, Joseph DD. *Elementary Stability and Bifurcation Theory*. New York: Springer, 1980.
43. Collins RT, Jones JJ, Harris MT, Basaran OA. Electrohydrodynamic tip streaming and emission of charged drops from liquid cones. *Nat Phys*. 2008;4:149–154.
44. Collins RT, Sambath K, Harris MT, Basaran OA. Universal scaling laws for the disintegration of electrified drops. *Proc Natl Acad Sci USA*. 2013;110(13):4905–4910.

Manuscript received Dec. 13, 2013.